Dirac gap-induced graphene quantum dot in an electrostatic potential

G. Giavaras[1] and Franco Nori[1,2]

[1]*Advanced Science Institute, RIKEN, Wako-shi, Saitama 351-0198, Japan*

[2]*Department of Physics, The University of Michigan, Ann Arbor, Michigan 48109-1040, USA*

(Received 26 January 2011; revised manuscript received 11 February 2011; published 19 April 2011)

A spatially modulated Dirac gap in a graphene sheet leads to charge confinement, thus enabling a graphene quantum dot to be formed without the application of external electric and magnetic fields [G. Giavaras and F. Nori, Appl. Phys. Lett. **97**, 243106 (2010)]. This can be achieved provided the Dirac gap has a local minimum in which the states become localized. In this work, the physics of such a gap-induced dot is investigated in the continuum limit by solving the Dirac equation. It is shown that gap-induced confined states couple to the states introduced by an electrostatic quantum well potential. Hence the region in which the resulting hybridized states are localized can be tuned with the potential strength, an effect which involves Klein tunneling. The proposed quantum dot may be used to probe quasirelativistic effects in graphene, while the induced confined states may be useful for graphene-based nanostructures.

DOI: 10.1103/PhysRevB.83.165427 PACS number(s): 73.21.La, 73.23.−b, 81.05.ue

I. INTRODUCTION

Quantum dots have been studied extensively over the last years because they allow fundamental laws of quantum physics to be probed and they might also find applications in nanoelectronics as detectors and transistors. Although a dot in a semiconductor heterostructure can be routinely formed, in monolayer graphene the situation is different.[1–4] An ideal graphene sheet is gapless, its energy dispersion is linear $E = \pm v_F|\mathbf{p}|$, and its charge carriers are massless Dirac particles. Therefore, they exhibit Klein tunneling, which allows massless particles to tunnel through any electrostatic potential barrier. This property excludes the possibility of fabricating a graphene dot simply by using electrostatic gates, as in common semiconductors.

In particular, the states of an electrostatic graphene dot are deconfined, that is, they have an oscillatory tail outside the dot region, which is a direct consequence of the Klein tunneling.[5–7] This essentially means that the electrons can only spend a finite time interval inside the dot, and it has been shown theoretically that this time interval is sensitive to the details of the potential profile and the energy of the quantum state.[7] A uniform magnetic field leads to confined states (bound states) which decay exponentially outside the dot, provided the electrostatic potential rises slowly compared to the magnetic vector potential.[8,9] Thus a graphene quantum dot can be formed with a uniform magnetic field. This property has also potential applications in graphene waveguides.[10,11]

It is experimentally possible to induce an energy gap in graphene's band structure, referred to as the Dirac gap.[1,2] In this case the energy dispersion becomes $E = \pm\sqrt{(v_F\mathbf{p})^2 + \Delta^2}$, with 2Δ the value of the Dirac gap. The importance of the gap stems from the fact that it gives rise to carriers with mass ($\sim\Delta/v_F^2$) and thus a quantum well potential induces confinement as in common semiconductor dots.[1,2] This happens because the Klein tunneling is suppressed for a particle with mass, as long as its energy lies in the gap. The quantum states with energies within the gap decay exponentially in the barrier region, thus trapping the electron in the dot for a theoretically infinite time.

This work considers the case of a spatially modulated Dirac gap that enables a graphene quantum dot to be formed without the application of external electric and magnetic fields.[12] This is feasible provided the gap has a local minimum in which the electron states become localized. Gap-induced confined states couple with states induced by an electrostatic quantum well potential; then this property allows the region in which the resulting hybridized states are localized to be tuned with the potential strength. This type of dot can be used to probe quasirelativistic effects in graphene, related to Klein tunneling, while the confined states may be useful for applications. To manipulate the spin states of an electron confined in a quantum dot, magnetic fields are usually needed. Thus, forming a graphene dot without applying additional magnetic fields to control the charge states can be advantageous. This is one of the motivations of our proposal. Moreover, the density of states in a gap-induced dot can be made low enough since only states with energies in the gap are of importance. A magnetic dot does not have this property and it is more tricky to induce a low density of states.[13]

The value of the Dirac gap depends on the specific experimental technique and can range from a few to hundreds of meV. For example, a Dirac gap has been measured in graphene grown epitaxially on a SiC substrate.[14] A gap opening has been demonstrated by controlling the structure of the interface between graphene and ruthenium.[15] Further, a spatially modulated and (buffer layer) thickness-dependent Dirac gap has been reported experimentally.[16] Moreover, it has been suggested theoretically that local strain and/or chemical methods might also be employed to open up and tune the Dirac gap.[1,2,17–19]

This paper is organized as follows. In Sec. II the quantum dot model is presented and the necessary conditions for confinement are derived in the presence of a magnetic vector and scalar potentials, as well as a spatially modulated Dirac gap. In Sec. III a model dot is examined in the regime where the Dirac gap has the same spatial profile as the electrostatic potential. In Sec. IV some semianalytical results are derived for the case of a piecewise-constant Dirac gap profile and the general properties of the gap-induced dot are presented. The

interplay of the gap-induced dot with an electrostatic quantum well potential is studied in Sec. V, and Sec. VI presents the basic conclusions of the paper.

II. PHYSICAL MODEL

A. Graphene quantum dot Hamiltonian

For energies near the Dirac points ($<\pm 1$ eV) and in the continuum limit, a graphene quantum dot can be described by the effective 2×2 Hamiltonian

$$H = v_F \boldsymbol{\sigma} \cdot (\mathbf{p} + e\mathbf{A}) + V\mathcal{I} + \tau\Delta\sigma_z. \tag{1}$$

The Fermi velocity $v_F = \gamma/\hbar$ is assumed to be position independent, where $\gamma = 646$ meV nm is a band structure parameter. Also, $\boldsymbol{\sigma} = (\sigma_x, \sigma_y)$, σ_z are the 2×2 Pauli operators acting on the two carbon sublattices, $\mathcal{I}$ is the 2×2 unit matrix, $\mathbf{p} = -i\hbar\boldsymbol{\nabla} = -i\hbar(\partial_x, \partial_y)$ is the two-dimensional momentum operator, $\mathbf{A}$ is the vector potential that generates the magnetic field $\mathbf{B} = \boldsymbol{\nabla} \times \mathbf{A}$, and V is the quantum well potential formed electrostatically, for example, due to a gate voltage. The last term in Eq. (1), referred to as the mass term, gives rise to an energy gap 2Δ in the spectrum of graphene, where $\tau = +1$ ($\tau = -1$) corresponds to the K (K') valley. The Hamiltonian (1) assumes no intervalley coupling, which is a good approximation for most graphene samples.[1,2]

For the dot model we consider that both V and Δ have cylindrical symmetry and the applied magnetic field is perpendicular to the graphene sheet (i.e., $\mathbf{B} = B\hat{z}$). Hence only the azimuthal component A_θ is nonzero, therefore

$$\mathbf{A} = (0, A_\theta, 0), \quad A_\theta = \frac{B_0 r^s}{s+1}, \tag{2}$$

which generates the field $B = B_0 r^{s-1}$; here, $s = 1$ corresponds to a uniform magnetic field. Hamiltonian Eq. (1) is written in cylindrical coordinates ($x = r\cos\theta$, $y = r\sin\theta$) with the substitution

$$\partial_x - i\,\partial_y = e^{-i\theta}\left(\partial_r - \frac{i}{r}\partial_\theta\right), \tag{3}$$

and

$$\boldsymbol{\sigma} \cdot \mathbf{A} = -(\sigma_x \sin\theta - \sigma_y \cos\theta)A_\theta. \tag{4}$$

A two-component solution Ψ to the Dirac equation

$$H\Psi = E\Psi, \tag{5}$$

with E being the eigenenergy, is written in the general form

$$\Psi = \frac{1}{\sqrt{r}}\begin{pmatrix} f_1(r)\exp[i(m-1)\theta] \\ i f_2(r)\exp(im\theta) \end{pmatrix}, \tag{6}$$

with $m = 0, \pm 1, \ldots$, being the orbital angular momentum quantum number. The radial components f_1 and f_2 express amplitude probabilities on the two carbon sublattices of graphene, and they satisfy the two coupled differential equations

$$(V + \tau\Delta)f_1 + \left(U + \gamma\frac{d}{dr}\right)f_2 = Ef_1, \tag{7a}$$

$$\left(U - \gamma\frac{d}{dr}\right)f_1 + (V - \tau\Delta)f_2 = Ef_2. \tag{7b}$$

The term U is due to the angular momentum and the applied magnetic field, and is given by

$$U = \frac{\gamma(2m-1)}{2r} + \frac{\gamma e A_\theta}{\hbar}. \tag{8}$$

Applying the time-reversal symmetry operator $i\mathcal{C}\sigma_y$, with $\mathcal{C}$ the operator of complex conjugation, to Eqs. (7a) and (7b), it can be shown that the eigenenergies[20] satisfy the condition $E(m, B, \tau) = E(1-m, -B, -\tau)$. Also, $E(V, \tau) = -E(-V, -\tau)$ due to electron-hole symmetry.

B. Confinement in a Dirac gap-induced dot

The quantum states of a Schrödinger dot, formed by an electrostatic quantum well, can be classified according to their energy. A state is confined when its energy relative to the bottom of the well is smaller than the well depth. This state has an exponential tail at a large distance from the quantum well. In the opposite regime, when the energy is larger than the well depth, the state is deconfined and it has an oscillatory tail.

This behavior is no longer valid for a Dirac dot formed in graphene because the energy spectrum of graphene is unbound and Klein tunneling takes place. In particular, a massless Dirac electron can tunnel through any electrostatic potential barrier, as has been confirmed experimentally via transport measurements in p-n junctions.[21] For this reason an electrostatic graphene dot cannot confine electrons.

Nevertheless, confinement can be achieved in the presence of a magnetic field and/or an energy gap in graphene's spectrum, though for this to happen some specific conditions have to be satisfied, which are analyzed in this section. As a general rule, confined states should decay asymptotically [i.e., at a large ($r \to \infty$) radial distance r, independent of their energy], whereas deconfined states should have an oscillatory tail. The former states are sometimes called bound and the latter quasibound.

Below we employ a rigorous treatment to examine the dot states.[8] We derive a single second-order differential equation for each radial component, by decoupling Eqs. (7a) and (7b). Then we identify the form of the state in the asymptotic region (i.e., at a large radial distance from the origin of the dot). The f_2 component satisfies

$$\frac{d^2 f_2}{dr^2} + a(r)\frac{df_2}{dr} + b(r)f_2 = 0, \tag{9}$$

with the coefficients

$$a(r) = -\frac{V_+'}{V_+ - E},$$

and

$$b(r) = a\frac{U}{\gamma} - \frac{U^2}{\gamma^2} + \frac{(V_- - E)(V_+ - E)}{\gamma^2} + \frac{U'}{\gamma},$$

with $V_\pm = V \pm \tau\Delta$ and the prime denotes differentiation with respect to r. The first derivative term in Eq. (9) complicates the analysis of the quantum states. For this reason we eliminate it by writing f_2 in the form $f_2(r) = g(r)u_2(r)$ and from Eq. (9) we derive that

$$g\frac{d^2 u_2}{dr^2} + (2g' + ag)\frac{du_2}{dr} + (g'' + ag' + bg)u_2 = 0. \tag{10}$$

If we choose $g = \exp(-\int a/2dr)$, the first derivative term cancels and u_2 satisfies the Schrödinger-like equation

$$\frac{d^2u_2}{dr^2} + k_2^2(r)u_2 = 0, \tag{11}$$

with the r-dependent coefficient

$$k_2^2(r) = b - \frac{1}{2}\frac{da}{dr} - \frac{a^2}{4}. \tag{12}$$

Here g is not an oscillatory function of r, therefore f_2 has the same confined or deconfined character as u_2. Specifically, Eq. (11) suggests that u_2 is confined only if k_2^2 is asymptotically ($r \to \infty$) negative. Otherwise u_2 is deconfined. The same arguments are valid for the f_1 component.[22]

To proceed, we assume that for a large radial distance r both V and Δ are constant or have a power-law dependence; therefore in this case we derive asymptotically that

$$k_2^2(r) \approx -\left(\frac{eA_\theta}{\hbar}\right)^2 + \left(\frac{V-E}{\gamma}\right)^2 - \left(\frac{\tau\Delta}{\gamma}\right)^2. \tag{13}$$

Equation (13) shows that the sign of k_2^2 is tunable with A_θ, V, Δ, and energy E, and thus the same is valid for the character of the dot states. Further, the character of the states is independent of the choice of valley $\tau = \pm 1$, although for a fixed m the energies are not the same for both valleys.

The form of $k_2^2(r)$ in Eq. (13) shows that the vector potential acts equivalently to the mass term, namely, both have the tendency to confine the states. This can be understood as follows. It can be seen from Eqs. (7a) and (7b) that the radial Hamiltonian which acts on f_1 and f_2 is

$$H_r = \begin{pmatrix} V + \tau\Delta & U - \gamma\frac{d}{dr} \\ U + \gamma\frac{d}{dr} & V - \tau\Delta \end{pmatrix}. \tag{14}$$

The similarity transformation $P^\dagger H_r P = \mathcal{H}_r$ with the operator

$$P = \frac{1}{\sqrt{2}}\begin{pmatrix} 1 & 1 \\ 1 & -1 \end{pmatrix}, \tag{15}$$

results in the transformed Hamiltonian

$$\mathcal{H}_r = \begin{pmatrix} V + U & \tau\Delta + \gamma\frac{d}{dr} \\ \tau\Delta - \gamma\frac{d}{dr} & V - U \end{pmatrix}. \tag{16}$$

Among the terms which dominate asymptotically, U and $\tau\Delta$ are interchanged in $\mathcal{H}_r$ with respect to H_r. However, asymptotically $U \sim \gamma eA_\theta/\hbar$, therefore in this regime $\tau\Delta$ and A_θ should act equivalently.

The necessary condition for the occurrence of confinement (i.e., $k_2^2 < 0$ asymptotically) means that at least one of A_θ, Δ has to be nonzero, otherwise $k_2^2 > 0$ leading to deconfined states. Most importantly, Eq. (13) shows that confined states can be induced even for $A_\theta = 0$ and $V = 0$ everywhere, provided that $E^2 - \Delta^2 < 0$ asymptotically. As shown in Ref. 12 this inequality can be satisfied when Δ is spatially dependent; for example, when Δ is zero within a disk area, and nonzero outside that area, $\Delta = \delta_0$. Then, as shown below, discrete energy levels in the range $|E| < \delta_0$ correspond to confined states with a large amplitude within the disk area.

III. MODEL QUANTUM DOT SYSTEM

To demonstrate the arguments presented in the previous section, consider first a model quantum dot for which the electrostatic potential V, and the mass term Δ have a power-law spatial dependence. Equation (13) shows that if $A_\theta = 0$, and V, Δ are unequal, then confined states occur only if $(V - \Delta) < 0$, so that $k_2^2 < 0$. In this case confinement is energy independent (i.e., all the states independent of their energy are confined). In the special limit of $V = \Delta$ only energies which satisfy $-EV < 0$ correspond to confined states, which implies that if V increases (decreases) asymptotically then confinement occurs only for positive (negative) energies.

The complete physical behavior can be demonstrated when V and Δ have the same r dependence, for example, parabolic, $V = V_0 r^2$ and $\Delta = \Delta_0 r^2$ with $V_0, \Delta_0 > 0$. Then from Eq. (13) the resultant states are confined when $\Delta_0 > V_0$ so that $k_2^2 < 0$, and deconfined when $\Delta_0 < V_0$ and hence $k_2^2 > 0$. For $V_0 = \Delta_0$ only positive energies correspond to confined states.

To quantify this behavior the two coupled Eqs. (7a) and (7b) are discretized on a uniform grid and the resulting matrix eigenvalue problem is solved numerically, using a similar technique as in Ref. 8. The boundary conditions for the components f_1 and f_2 which lead to a Hermitian eigenvalue problem [Eqs. (7a) and (7b)] are derived in Ref. 8, and it can be shown that these are not modified by the presence of the mass term. So one component has to vanish at the origin and the second has to vanish asymptotically (at the boundary of the computational box). The same procedure is followed in all sections.

Figure 1 shows quantum states for Δ_0 constant, $\Delta_0 = 1\ \mu\text{eV nm}^{-2}$, and three different choices of V_0. The states plotted are those which correspond to the lowest positive energy when $V_0 = 0$. When $V_0 = 0$ ($< \Delta_0$) the states are confined and they have an exponential tail. This demonstrates that a graphene dot can be formed thanks to a spatially modulated Dirac gap without applying external electric or magnetic fields. When $V_0 = 0.9\Delta_0$ ($< \Delta_0$) the states are still confined though the region within which they are localized is slightly modified by the presence of the potential. On the other hand, when $V_0 = 1.5\Delta_0$ ($> \Delta_0$) the states have undergone a transition and they are deconfined asymptotically with an oscillatory tail. This behavior of the states with respect to the potential strength is valid for all values of m and $\tau = \pm 1$; though, as shown in Fig. 1, the relative amplitude of the two components depends on the choice of τ. In particular, for $\tau = +1$, $f_1 > f_2$ ($f_1 < f_2$) when $E > 0$ ($E < 0$), whereas the opposite is valid for $\tau = -1$, $f_1 < f_2$ ($f_1 > f_2$) when $E > 0$ ($E < 0$) (Ref. 23).

A similar confinement-deconfinement transition in the character of the dot states can also be induced for $\Delta = 0$, provided that the vector potential is nonzero ($A_\theta \neq 0$) and has the same power-law dependence as the electrostatic potential.[8] This can happen because the first and third terms in Eq. (13) have the same sign. This observation might be the key to fabricate a graphene dot with the help of a uniform magnetic field and an electrostatic potential, and some preliminary calculations suggest that this should be feasible in realistic dot designs formed in gated graphene.[8,24]

Figure 2 shows the energy level diagram in a range of confined states for the two valleys $\tau = \pm 1$. The spectrum

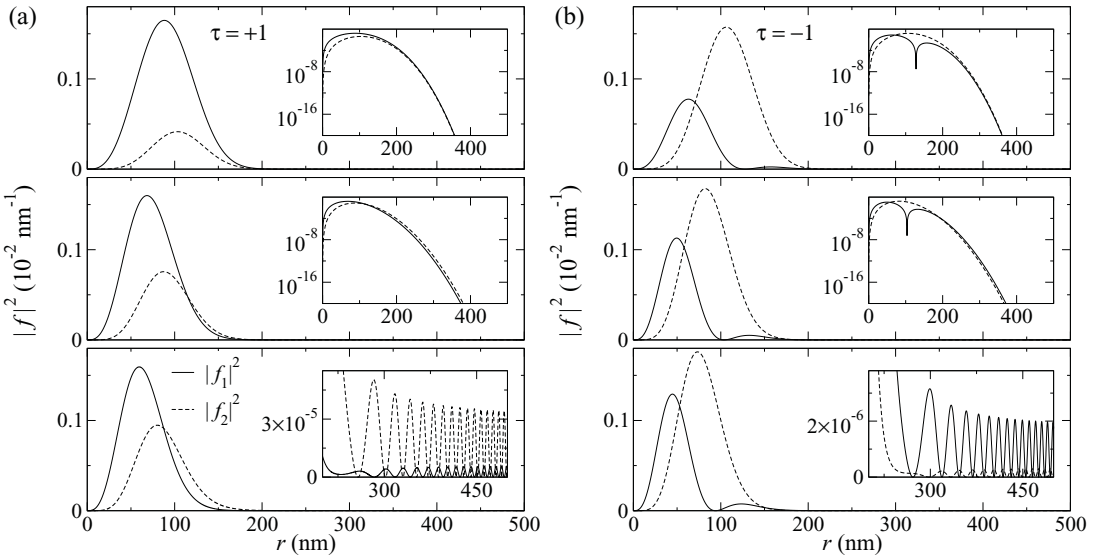

FIG. 1. (a) Quantum states for $m = 2$, $\tau = +1$ and different potential strengths V_0. The mass term is modelled by $\Delta = \Delta_0 r^2$, with $\Delta_0 = 1\ \mu$eV nm^{-2}, and the electrostatic potential is modelled by $V = V_0 r^2$. The potential strength V_0 is from top to bottom: $V_0/\Delta_0 = 0$, 0.9, and 1.5. The vertical axes of the insets to the top and middle panels are on logarithmic scale. (b) As in (a) but for $\tau = -1$.

consists of two ladders (sets) of discrete levels indicating the existence of confined states. The energy ladders are separated by a gap which is large when the angular momentum is large. As V_0 increases the confinement for negative energies becomes weak and for this reason the splitting between the discrete levels cannot be clearly resolved. The pattern of the two ladders is characteristic of confined states in graphene quantum dots and, for instance, can also occur when the mass term is replaced by a vector potential of the same spatial dependence.[24]

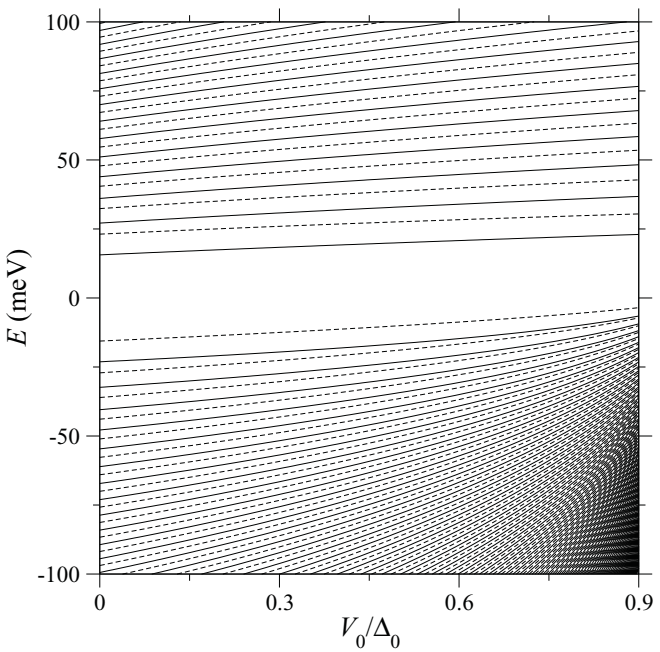

FIG. 2. Energy levels of confined states for the two valleys: $\tau = +1$ (solid lines) and $\tau = -1$ (dashed lines). The angular momentum number is $m = 2$, the electrostatic potential is modelled by $V = V_0 r^2$ and the mass term is modelled by $\Delta = \Delta_0 r^2$. Here $\Delta_0 = 1\ \mu$eV nm^{-2}, whereas V_0 is tuned.

IV. INVESTIGATION OF A DIRAC GAP-INDUCED DOT

In this section the basic properties of a Dirac gap-induced dot are investigated numerically. We assume that there is neither an electrostatic potential ($V = 0$) nor a magnetic field ($A_\theta = 0$) and thus confinement is due solely to the spatial modulation of the gap. Then confinement depends on energy, as can be seen from Eq. (13), and it is achieved when $E^2 - \Delta^2 < 0$, where Δ is the value of the mass term asymptotically.

A. Graphene dot formed by a piecewise-constant Dirac gap

First a regime for which analytical results can be obtained is examined. Consider the special limit where the spatially dependent mass term Δ changes discontinuously. In this case Δ can be modelled by the expression

$$\Delta(r) = \delta_0 \Theta(r - R), \tag{17}$$

with Θ the Heaviside step function. For simplicity we assume that $\Delta(r) = 0$ for $r < R$, although in the following analysis a nonzero value can be introduced straightforwardly. As shown in the previous section, the two radial components f_1 and f_2 satisfy a second-order differential equation, which for $V = 0$ and $A_\theta = 0$ has the form [$(\tau\Delta)^2 = \Delta^2$]

$$\frac{d^2 f_1}{dr^2} - \frac{4(m-1)^2 - 1}{4r^2} f_1 + \frac{E^2 - \Delta^2}{\gamma^2} f_1 = 0, \tag{18a}$$

$$\frac{d^2 f_2}{dr^2} - \frac{4m^2 - 1}{4r^2} f_2 + \frac{E^2 - \Delta^2}{\gamma^2} f_2 = 0. \tag{18b}$$

If we assume a solution of the form $f_i = \sqrt{r}\mathcal{F}_i$, then $\mathcal{F}_i$ has to satisfy the following Bessel's differential equations

$$\frac{d^2\mathcal{F}_1}{dr^2} + \frac{1}{r}\frac{d\mathcal{F}_1}{dr} - \frac{(m-1)^2}{r^2}\mathcal{F}_1 + \frac{E^2-\Delta^2}{\gamma^2}\mathcal{F}_1 = 0, \quad (19a)$$

$$\frac{d^2\mathcal{F}_2}{dr^2} + \frac{1}{r}\frac{d\mathcal{F}_2}{dr} - \frac{m^2}{r^2}\mathcal{F}_2 + \frac{E^2-\Delta^2}{\gamma^2}\mathcal{F}_2 = 0. \quad (19b)$$

Setting $k = E/\gamma$ and $q = \sqrt{|E^2-\delta_0^2|}/\gamma$, the solutions for confined states can be written in the general form

$$\begin{pmatrix}\mathcal{F}_1\\ \mathcal{F}_2\end{pmatrix} = \begin{pmatrix}\alpha J_{m-1}(kr)\\ \alpha J_m(kr)\end{pmatrix}, \quad r \leqslant R, \quad (20)$$

and

$$\begin{pmatrix}\mathcal{F}_1\\ \mathcal{F}_2\end{pmatrix} = \begin{pmatrix}\beta K_{m-1}(qr)\\ c\beta K_m(qr)\end{pmatrix}, \quad R \leqslant r, \quad (21)$$

with $c = \sqrt{|E^2-\delta_0^2|}/(E+\tau\delta_0)$ and α, β are constants that can be determined from the normalization condition and the requirement that both components are continuous at $r = R$. Here J_m is an ordinary Bessel function of the first kind, and K_m is a modified Bessel function of the second kind. These have been chosen since J_m is regular at the origin ($r = 0$), while K_m decays exponentially at large radial distances as needed for confined states.[25] The coefficients (α,β,c) in Eqs. (20) and (21) are introduced in order f_1 and f_2 to satisfy the coupled Eqs. (7a) and (7b).

Both components have to be continuous at $r = R$, leading to the following algebraic equation

$$cJ_{m-1}(kR)K_m(qR) = J_m(kR)K_{m-1}(qR). \quad (22)$$

This is solved numerically, with bisection, to give the energies of the confined states in the range $|E| < \delta_0$. Thanks to the properties of the Bessel functions $J_{-m} = (-1)^m J_m$ and $K_{-m} = K_m$, the energies satisfy the condition $E(m,\tau) = E(1-m,-\tau)$ as time-reversal symmetry requires when $A_\theta = 0$. Figure 3 shows one example of the two confined components for the lowest positive energy. When this is much smaller than δ_0 the states decay quickly in the region $r > R$, while the states exhibit a kink at $r = R$ because their first derivative is discontinuous at that point.

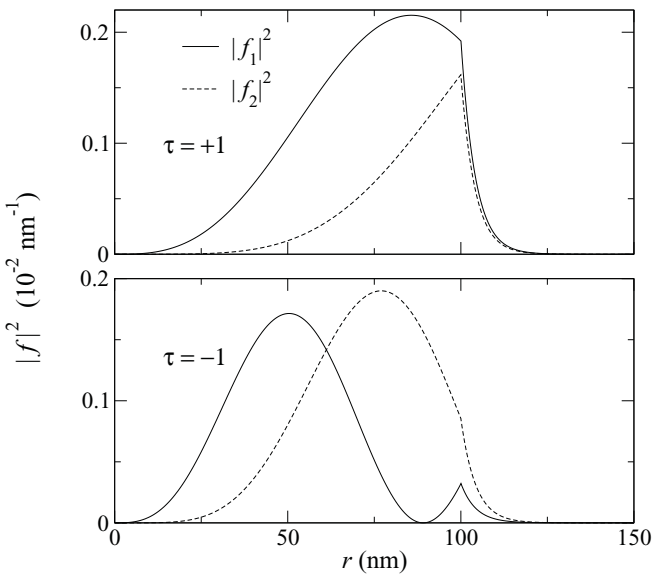

FIG. 3. Quantum states for a piecewise-constant mass term Δ given by Eq. (17). The parameters are $m = 2$, $R = 100$ nm, and $\delta_0 = 80$ meV. Results for both valleys, $\tau = \pm 1$, are shown. The states correspond to the lowest positive eigenenergy.

B. Graphene dot formed by a continuous Dirac gap profile

In any realistic graphene system the spatial modulation of the Dirac gap will not be perfectly sharp. For this reason we make a more realistic choice of the mass term than that in Eq. (17) and use the expression

$$\Delta(r) = \begin{cases} 0, & r \leqslant R, \\ -\delta_0 \cosh\left(\frac{r-R}{d}\right)^{-2} + \delta_0, & R \leqslant r, \end{cases} \quad (23)$$

so that asymptotically $\Delta \approx \delta_0$. For all the calculations we choose for the parameters $R = 250$ nm and $d = 150$ nm, although these choices do not affect the main conclusions. In the limit $d \to 0$ we recover Eq. (17).

Figure 4 shows the energy levels as a function of the asymptotic value of the mass term δ_0, giving rise to an energy gap of $2\delta_0$. The (quasi) continuum of levels, corresponding to the black area in Figs. 4(a) and 4(b), reflect deconfined states. The finite system size needed for the numerical calculations generates a gap at $\delta_0 = 0$, which increases with $|m|$. However, the system size is chosen large enough and hence it does not affect the physics of the discrete levels of the dot that we are interested in. These levels emerging through the continuum reflect the formation of confined states. The transition from continuum to discrete levels and vice versa is accompanied by the appearance of anticrossing points.[12] As seen in Figs. 4(a) and 4(b), the discrete levels form two ladders (sets) of energy with either positive or negative values, separated by a gap pertinent to the angular motion. The typical splitting of the levels increases with δ_0 because the confinement becomes stronger. Further, the two energy ladders are formed after a critical value of δ_0 depending on the angular momentum. This happens because the angular motion tends to delocalize the states near the origin of the dot, see Eq. (8), and therefore for a given δ_0 not all m values produce confined states. For this reason there are no discrete levels for $\delta_0 \lesssim 3$ and 28 meV in Fig. 4, when $m = 2$ and $m = 15$, respectively.

If $|m|$ is large, then δ_0 has to be large for the formation of confined states. This effect has a direct signature in the density of states (DOS) which is shown in the contour plot of Fig. 4(c). For simplicity only $\tau = +1$ is considered since the inclusion of $\tau = -1$ simply doubles the number of states. Moreover, because $V = A_\theta = 0$ the energies satisfy the condition $E(m,\tau) = -E(1-m,\tau)$ and thus the DOS is symmetric with respect to $E \to -E$. For a small δ_0 only a few energy levels near zero lie within the gap, corresponding to small angular momentum states. The general trend is that with increasing δ_0 the number of discrete levels that falls in the gap increases since gradually larger m values give confined states. As an example, for $\delta_0 = 5$ meV the discrete levels correspond to angular momentum numbers $-1 \leqslant m \leqslant 2$, whereas for $\delta_0 = 20$ meV to $-9 \leqslant m \leqslant 10$. Still, however, for energies

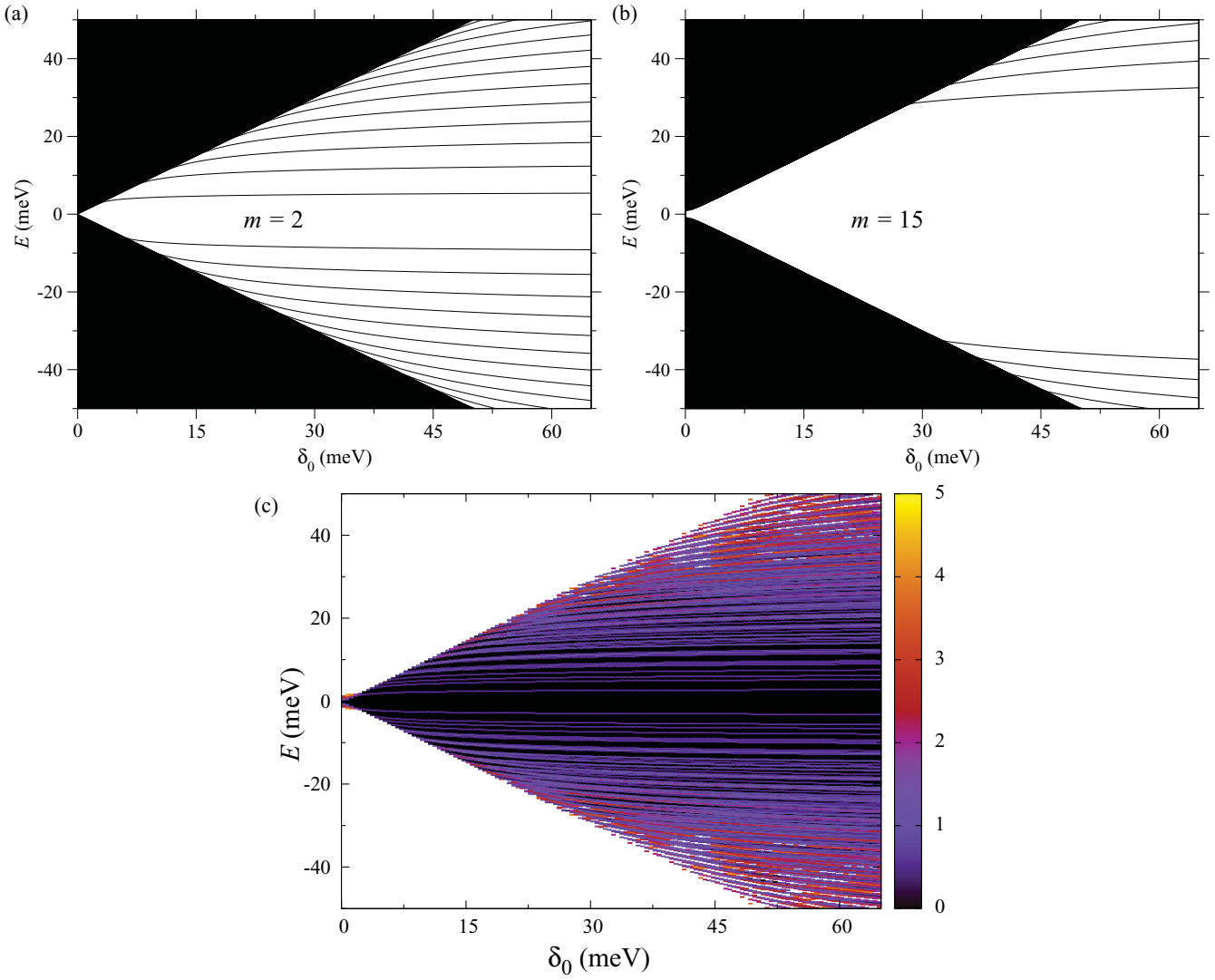

FIG. 4. (Color online) (a), (b) Energy levels, for $\tau = +1$, as a function of the asymptotic value of the mass term δ_0 which generates a Dirac gap of $2\delta_0$. The mass term Δ is modelled by Eq. (23). (c) The contour plot shows the density of states; the maximum number of states is restricted to five.

near the middle of the Dirac gap, -5 meV $\lesssim E \lesssim 5$ meV, the DOS remains low regardless of δ_0 because only small m values contribute to this energy range. This suggests that the formation of a gap-induced dot can be probed using similar charge measurements as, for example, in GaAs dots. The Fermi energy of the graphene dot has to be adjusted near the middle of the energy gap where the DOS is expected to be low and scanning tunneling microscopy could be used to probe the confined quantum states.

V. EFFECT OF A QUANTUM WELL POTENTIAL ON A GAP-INDUCED DOT

In this section the effect of an electrostatic quantum well potential on a gap-induced dot is examined. It is assumed that the potential can be generated by a gate electrode and is not related to the presence of the Dirac gap. We consider the most common experimental regime where both the electrostatic potential V and the mass term Δ are constant asymptotically. In this case, if $A_\theta = 0$ then confinement depends on energy, as can be seen from Eq. (13), and it is achieved when $(V - E)^2 - \Delta^2 < 0$. If A_θ has a power-law dependence the states are always confined independent of their energy, but in this work we focus on the case where $A_\theta = 0$, and therefore there is no magnetic field in the graphene sample.

The interplay of a quantum well potential with the gap-induced dot has a drastic effect on the resulting states. In particular, gap-induced dot states couple to the states induced by the potential. As a result the region in which the resulting hybridized states are localized is tunable with the strength of the potential. Also, Klein tunneling in the electrostatic barrier region occurs.

It has been experimentally demonstrated that gate electrodes can be suspended above the graphene sheet inducing a smooth quantum well or barrier potential that is tunable with the applied gate voltage.[26,27] The exact potential profile can be determined by solving the Poisson equation within a semiclassical Thomas-Fermi model properly taking into account charge

screening effects and the specific electrode geometry.[8,27] However, a smooth and slowly varying potential can be modelled, to a good approximation, by the Gaussian expression.[8,24]

$$V(r) = -V_0 \exp\left(-\frac{r^2}{l_0^2}\right). \tag{24}$$

The parameters V_0 and l_0 model the effective depth and width of the quantum well potential, which are controlled by the geometry of and the applied voltage to the gate electrodes. Typical gate voltages of a few volts generate a potential well depth of some hundreds of meV, with an effective width of some hundreds of nm. This work is concerned only with the regime where the quantum well potential is formed inside the spatial region where $\Delta \lesssim \delta_0$, with Δ as in Eq. (23), therefore for all the calculations $l_0 = 180$ nm and $V_0 \leqslant 120$ meV.

The energy level diagram as a function of V_0 is shown in Fig. 5(a), for a spatially independent (constant) Dirac gap with $2\Delta = 50$ meV. Confined states have discrete energy levels that lie within the gap, whereas deconfined states form an upper and a lower band of (quasi) continuum of levels, for energies $E > \Delta$ and $E < -\Delta$, respectively. If V_0 is small, the angular momentum delocalizes the states; therefore confined states are formed after a critical value of V_0, that is ∼19 meV in Fig. 5(a). As V_0 increases, the number of discrete levels increases due to the stronger confinement. Energy levels emerge from the upper continuum into the gap, while the lowest discrete levels merge into the lower continuum via anticrossing points. These are formed inside the two bands as shown in Ref. 12. The quantum states undergo a transition from confined to deconfined and vice versa. Specifically, a confined state transits to a deconfined

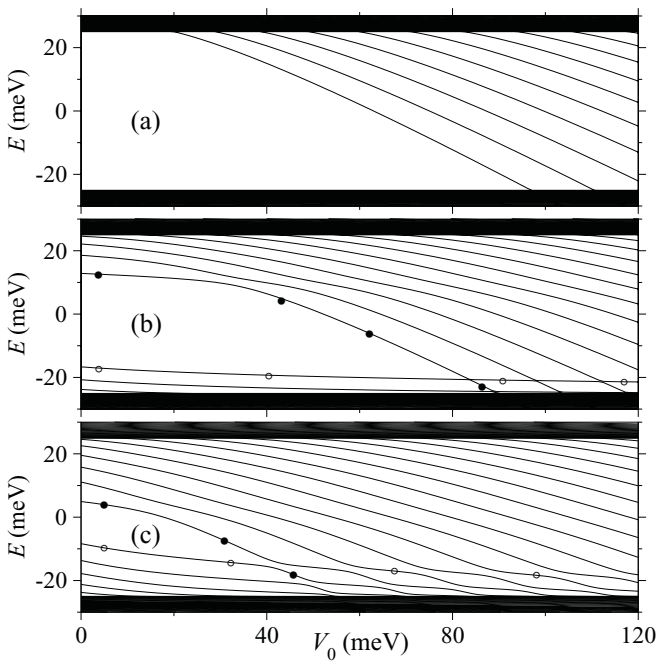

FIG. 5. (a) Energy levels versus the electrostatic potential depth V_0, for $m = 6$, $\tau = +1$ and a constant Dirac gap of $2\Delta = 50$ meV. (b) As in (a) but for a spatially modulated Dirac gap with an asymptotic value of $2\delta_0 = 50$ meV. (c) As in (b) but for $m = 2$. The states of the energies marked by circles are shown in Fig. 6.

via tunneling into the valence (lower) band, when its energy falls below the gap.[28] In this regime the deconfined state has an oscillatory tail but has a large amplitude near the origin of the dot (see below).

Figures 5(b) and 5(c) show the energy diagram when the Dirac gap is spatially modulated with an asymptotic value of $2\delta_0 = 50$ meV. The appearance of discrete levels for $V_0 = 0$ is a consequence of the gap-induced confinement. Such levels are absent in the constant gap system. Furthermore, for $V_0 = 0$ there are more discrete levels for $m = 2$ than $m = 6$, as expected based on the above arguments. Anticrossing points, formed now between discrete levels, indicate a coupling between potential- and gap-induced states. The gap-induced states of the upper energy ladder couple strongly to the potential states and for this reason the corresponding anticrossing points are not well formed. On the other hand, states of the lower energy ladder couple weakly to the electrostatic potential for $m = 6$ [Fig. 5(b)], and therefore the anticrossing points are well formed, while this coupling is much stronger for $m = 2$ [Fig. 5(c)].

Figure 6 illustrates the dot states as the potential depth V_0 increases. Consider first the $m = 2$ states shown in the left panels of Fig. 6(a). Confinement for $V_0 = 0$ is due to the spatial modulation of the Dirac gap and cannot be realized for a constant gap. As V_0 increases, the gap-induced state couples to the lowest energy state induced by the potential well ($V_0 =$ 30 meV), and its energy decreases. The state acquires a large amplitude in the potential well region and with increasing V_0 it couples successively to gap-induced states of the lower energy ladder ($V_0 = 50$ meV). In this range the resulting hybridized state is spread with significant amplitude over the whole nonasymptotic region defined by $\Delta \lesssim \delta_0$. Further increasing V_0, the energy of the state falls below the gap ($V_0 = 70$ meV); the state tunnels in the valence band and becomes deconfined with an oscillatory tail.

Strong coupling between gap- and potential-induced states occurs also for the $m = 2$ states shown in the right panels of Fig. 6(a); for instance, for $V_0 = 70$ and 100 meV. With increasing V_0, the gap-induced state that corresponds to the highest energy in the lower ladder (for $V_0 = 0$) couples successively to excited potential-induced states. This effect is reflected in the energy level diagram [Fig. 5(c)] by the appearance of a series of anticrossing points as V_0 increases. A similar effect is displayed by gap-induced states of smaller energy, although with increasing V_0 the number of gap-induced confined states in the lower energy ladder decreases. For instance, as seen in Fig. 5(c) for $V_0 = 0$ there are five discrete levels, whereas for $V_0 = 50$ meV there are three. The number of states can be determined using a similar approximate formalism as that in Ref. 9. The necessary condition for the existence of confined states is that there must be a spatial region near $r = R$ in which $k_2^2 > 0$, with k_2^2 as given in Eq. (12), whereas asymptotically $k_2^2 < 0$.

In Fig. 6(a) the coupling between potential- and gap-induced states of the lower ladder is strong and therefore the resulting hybridized states have a relatively strong amplitude over the whole region where $\Delta \lesssim \delta_0$. In contrast, the coupling is weak for the $m = 6$ states shown in Fig. 6(b). Therefore, for $V_0 = 85$ meV, the states peak mainly in the region defined either by the potential well (left panel) or the Dirac gap

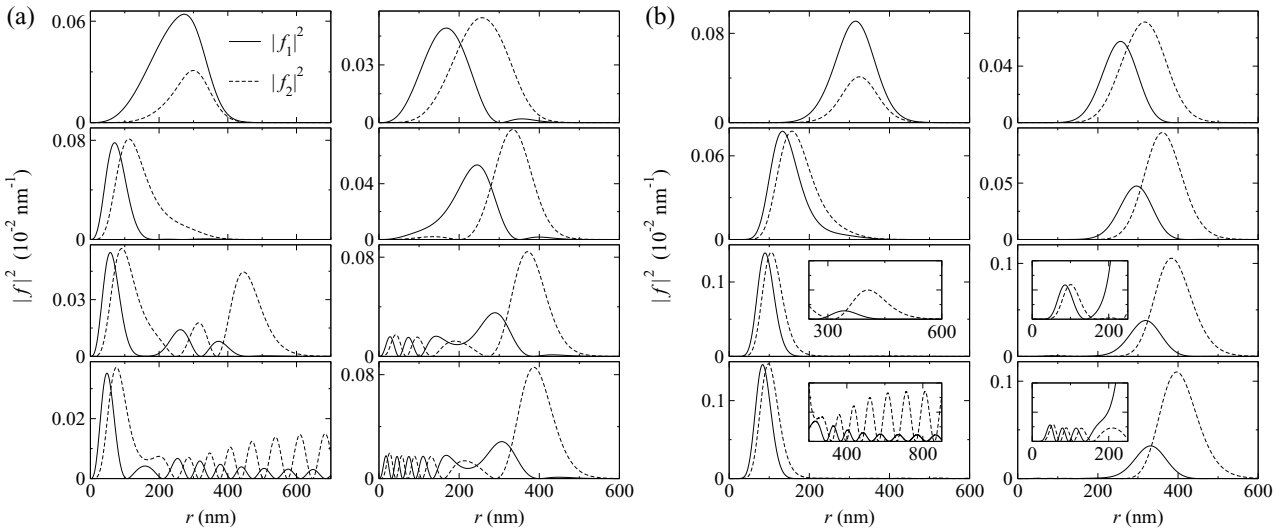

FIG. 6. (a) Quantum states for $m = 2$ and for different electrostatic potential depths V_0; from top to bottom: $V_0 = 0$, 30, 50, and 70 meV for the left panels, and $V_0 = 0$, 30, 70, and 100 meV for the right panels. The Dirac gap is spatially modulated with an asymptotic value of $2\delta_0 = 50$ meV. Left (right) panels show states with energies marked by • (○) in Fig. 5(c). (b) As in (a) but for $m = 6$ and $V_0 = 0$, 40, 85, and 100 meV for the left panels, and $V_0 = 0$, 40, 85, and 120 meV for the right panels. Left (right) panels show states with energies marked by • (○) in Fig. 5(b). The vertical axes of the insets range from 0 to 1×10^{-3}.

modulation (right panel). These two regions have a small overlap when m is large and the effective width of the potential well is smaller than the radius of the zero-gap region.

The m-dependent coupling of the states is related to the width of the classically forbidden region formed between the confinement regions defined by the gap modulation and the electrostatic well. The semiclassical approach developed in Ref. 6 shows that for a large positive m the width of the forbidden region is large. This results in a weak coupling between the potential- and gap-induced states of the lower energy ladder. Also, as m increases the gap between the upper and the lower energy ladders increases also (Fig. 4) and therefore V_0 has to be large for the formation of coupled states. The coupling effect, though, is insensitive to the details of the gap modulation. Our calculations show that both weak and strong couplings can be realized even when the Dirac gap changes discontinuously as in Eq. (17).

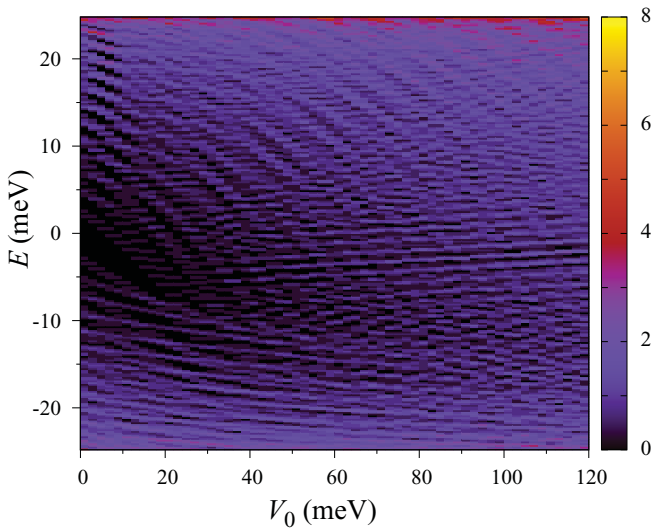

FIG. 7. (Color online) Density of states versus energy E ($|E| <$ 24.8 meV) and electrostatic potential depth V_0, for $\tau = +1$, and an asymptotic Dirac gap of $2\delta_0 = 50$ meV.

When the potential is nonzero ($V_0 \neq 0$) the induced states can have an oscillatory amplitude inside the barrier region, though asymptotically they decay.[29] This effect is a consequence of the Klein tunneling in the nonasymptotic region defined by $\Delta \lesssim \delta_0$. In contrast, the quantum states of a Schrödinger dot display only an exponential decay inside an electrostatic barrier. Numerical calculations of the DOS, shown in Fig. 7, suggest that it should be experimentally possible to resolve graphene states with large oscillatory amplitude in the barrier and the coupling between the states described above. To probe the states with scanning tunneling microscopy the DOS has to be low. This could be achieved for a small V_0 since in this case only energies that correspond to small m states fall in the gap. For the same reason the DOS is low when the asymptotic value of the Dirac gap is small.

VI. DISCUSSION AND CONCLUSION

The existence of a Dirac gap in the energy spectrum of monolayer graphene suppresses the Klein tunneling and thus enables charge confinement by an electrostatic quantum well and formation of quantum dots. Here it was shown that a graphene dot can be formed as a result of a spatially modulated Dirac gap. It was found, by solving the Dirac equation in the continuum limit, that when the gap has a local minimum confined states with discrete energy levels can be formed without applying external electric and/or magnetic fields. This cannot be achieved in a constant Dirac gap graphene system. The required gap modulation may be introduced with substrate engineering, local strain, or a chemical technique. Unlike quantum dots formed in nanocrystals of graphene, the proposed dot is formed in a large sheet of graphene, therefore the physics of the edges is unimportant and does not affect the dot properties.

The general conditions for confinement in the presence of a spatially modulated Dirac gap, an external electrostatic potential, and a magnetic vector potential were analyzed. When the gap and/or the vector potential rises asymptotically, while the electrostatic potential is zero (constant), the resulting states are confined regardless of angular momentum, valley and eigenenergy. The interplay of the gap-induced dot with an electrostatic potential leads to tunable quantum states (i.e., from confined to deconfined and vice versa). This can only happen provided the potential and the mass term, which generates the Dirac gap, have the same spatial forms asymptotically while the magnetic field is zero. In this case the states can be tuned with the strength of the potential: The states are deconfined when the electrostatic potential is stronger than the mass term and confined in the opposite regime.

When the Dirac gap is zero within a disk area and constant outside that area confinement is energy dependent, thus the choice of angular momentum and valley is important. Confined states are localized inside the disk area when their energies lie in the gap, otherwise the states are deconfined. The energy spectrum of the confined states consists of two ladders (sets) of discrete levels separated by a gap. Numerical calculations of the DOS suggest that states with small angular momentum lie in a region of low density and hence they could be probed using standard techniques such as scanning tunneling microscopy.

It was also shown that states induced by a quantum well potential, which may be generated by a gate electrode, can coexist and couple to gap-induced dot states. When the coupling is weak the states retain their character, whereas in the opposite regime the states are strongly hybridized. The signature of this coupling in the energy spectrum is the appearance of a series of anticrossing points. This coupling property offers a way of tuning the spatial region in which the hybridized states are localized with the strength of the potential. Moreover, the states can have a large oscillatory amplitude in the barrier region exhibiting Klein tunneling, before they eventually decay asymptotically. Calculations of the DOS indicate that these quasirelativistic effects could be probed.

ACKNOWLEDGMENTS

We thank P.A. Maksym for comments on the manuscript. G.G. acknowledges support from the Japan Society for the Promotion of Science (JSPS). F.N. acknowledges partial support from the Laboratory of Physical Sciences, National Security Agency, Army Research Office, AFOSR, DARPA, National Science Foundation Grant No. 0726909, JSPS-RFBR Contract No. 09-02-92114, Grant-in-Aid for Scientific Research (S), MEXT Kakenhi on Quantum Cybernetics, and Funding Program for Innovative R&D on S&T (FIRST).

[1] D. S. L. Abergel, V. Apalkov, J. Berashevich, K. Ziegler, and T. Chakraborty, Adv. Phys. **59**, 261 (2010).

[2] For an introductory review on mesoscopic graphene structures, see, for example, A. V. Rozhkov, G. Giavaras, Y. P. Bliokh, V. Freilikher, and F. Nori, Phys. Reports (2011) (in press).

[3] L. A. Ponomarenko, F. Schedin, M. I. Katsnelson, R. Yang, E. W. Hill, K. S. Novoselov, and A. K. Geim, Science **320**, 356 (2008).

[4] Quantum dots formed in nanoflakes of graphene have been fabricated (see Ref. 3), however, this work is concerned with dots formed in a large sheet of graphene, where the edges of the sheet have no effect on the dots properties and can be ignored.

[5] A. Matulis and F. M. Peeters, Phys. Rev. B **77**, 115423 (2008).

[6] H.-Yi Chen, V. Apalkov, and T. Chakraborty, Phys. Rev. Lett. **98**, 186803 (2007).

[7] P. Hewageegana and V. Apalkov, Phys. Rev. B **77**, 245426 (2008).

[8] G. Giavaras, P. A. Maksym, and M. Roy, J. Phys.: Condens. Matter **21**, 102201 (2009).

[9] G. Giavaras, P. A. Maksym, and M. Roy, Physica E **42**, 715 (2010).

[10] Y. P. Bliokh, V. Freilikher, and F. Nori, Phys. Rev. B **81**, 075410 (2010).

[11] Y. P. Bliokh, V. Freilikher, S. Savel'ev, and F. Nori, Phys. Rev. B **79**, 075123 (2009).

[12] G. Giavaras and F. Nori, Appl. Phys. Lett. **97**, 243106 (2010).

[13] P. A. Maksym, M. Roy, M. F. Craciun, M. Yamamoto, S. Tarucha, and H. Aoki, J. Phys.: Conf. Ser. **245**, 012030 (2010).

[14] S. Y. Zhou, G.-H. Gweon, A. V. Fedorov, P. N. First, W. A. de Heer, D.-H. Lee, F. Guinea, A. H. Castro Neto, and A. Lanzara, Nat. Mater. **6**, 770 (2007).

[15] C. Enderlein, Y. S. Kim, A. Bostwick, E. Rotenberg, and K. Horn, New. J. Phys. **12**, 033014 (2010).

[16] L. Vitali, C. Riedl, R. Ohmann, I. Brihuega, U. Starke, and K. Kern, Surf. Sci. **602**, 127 (2008).

[17] G. Giovannetti, P. A. Khomyakov, G. Brocks, P. J. Kelly, and J. van den Brink, Phys. Rev B **76**, 073103 (2007).

[18] R. P. Tiwari and D. Stroud, Phys. Rev. B **79**, 205435 (2009).

[19] R. M. Ribeiro, N. M. R. Peres, J. Coutinho, and P. R. Briddon, Phys. Rev. B **78**, 075442 (2008).

[20] The symbol $E(m,B,\tau)$ denotes the set of eigenergies given by Eqs. (7a) and (7b) for angular momentum number m, magnetic field B, and valley τ. The radial quantum number is not stated explicitly.

[21] A. F. Young and P. Kim, Nat. Phys. **5**, 222 (2009).

[22] The component f_1 satisfies a similar Schrödinger-like equation as f_2 but with $k_1^2 \neq k_2^2$. However, asymptotically $k_1^2 = k_2^2$.

[23] We are not concerned with a possible relative difference between the two components f_1 and f_2, but only with the relative maximum amplitude of the two components.

[24] G. Giavaras, P. A. Maksym, and M. Roy (unpublished).

[25] M. Boas, *Mathematical Methods in the Physical Sciences* (Wiley, New York, 2006).

[26] J. Velasco, Jr., G. Liu, W. Bao, and C. N. Lau, New J. Phys. **11**, 095008 (2009).

[27] R. V. Gorbachev, A. S. Mayorov, A. K. Savchenko, D. W. Horsell, and F. Guinea, Nano Lett. **8**, 1995 (2008).

[28] G. A. Steele, G. Gotz, and L. P. Kouwenhoven, Nat. Nanotech. **4**, 363 (2009).

[29] The barrier region for the states shown in Fig. 6 depends on the potential strength V_0 and the energy of the state. For example, for the state in Fig. 6(a) and $V_0 = 50$ meV (left panel) this region occurs for $r \gtrsim 170$ nm.